iScience, Volume *25*

Supplemental information

Chemical screen uncovers novel structural classes of inhibitors of the papain-like protease of coronaviruses

Kwiwan Jeong, Jinhee Kim, JuOae Chang, Subin Hong, Inseo Kim, Sunghyun Oh, Sangeun Jeon, Joo Chan Lee, Hyun-Ju Park, Seungtaek Kim, and Wonsik Lee

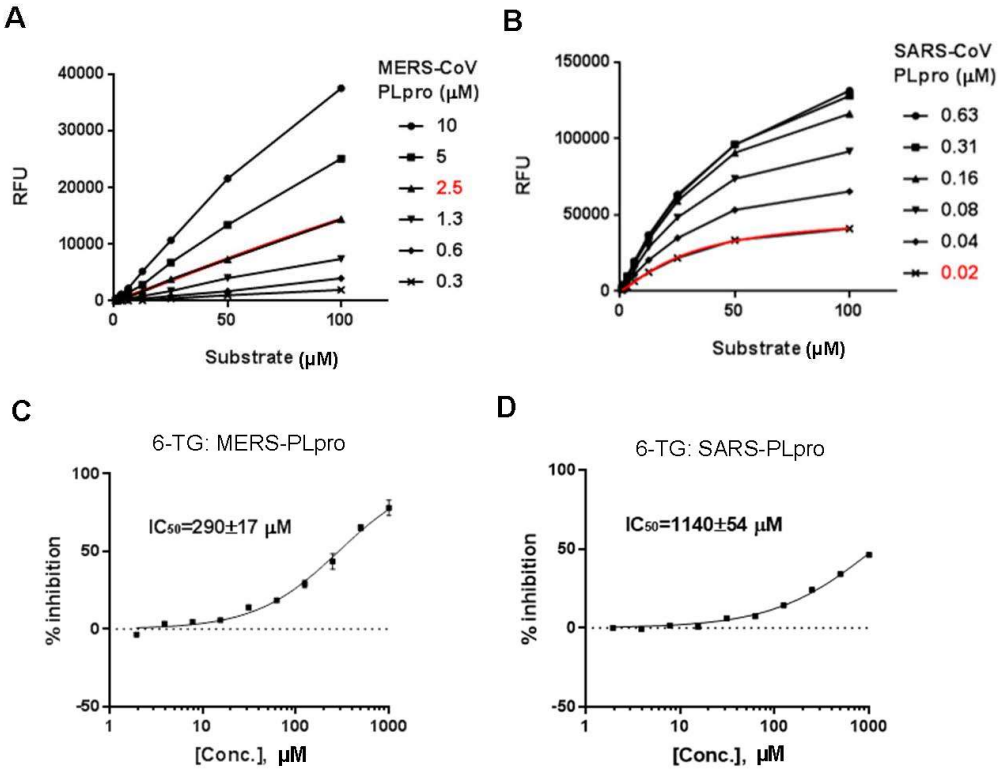

Figure S1. Optimization of fluorescence-based PLpro protease assay (related to Figure 1 and Figure 3). **(A, B)** Identification of optimal substrate and MERS-PLpro **(A)** and SARS-PLpro **(B)** enzyme concentrations for screening at room temperature. **(C, D)** Validation of selected substrate and enzyme concentrations using a known PLpro inhibitor 6-TG on MERS-PLpro **(C)** and SARS-PLpro **(D)**. Each data point represents the mean of duplicate assays with ±SEM.

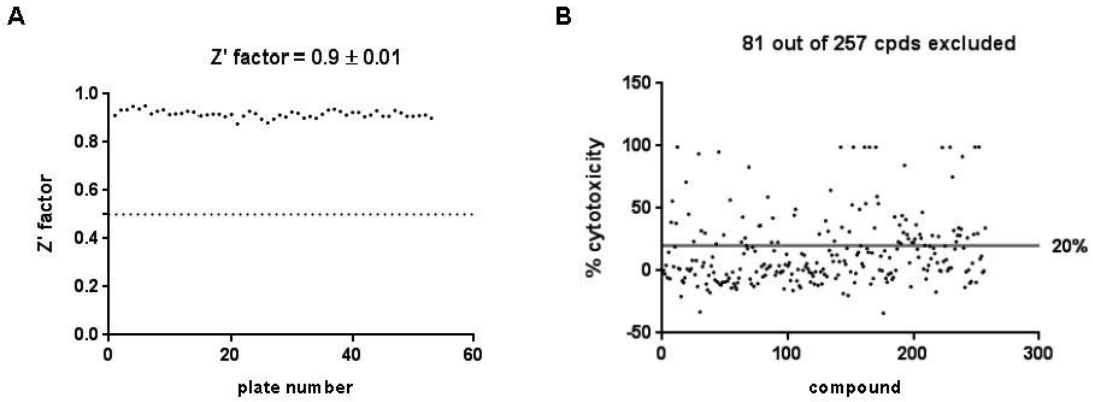

Figure S2. Z` factor of the compound screen and exclusion of cytotoxic compounds (related to Figure 1).
(A) Z'-factors of 60 assay plates. Average Z`-factor of 60 assay plates was calculated to be 0.91±0.01. **(B)** Cytotoxicity profile of primary hits. A total of 81 compounds from 257 primary hits were excluded by the cytotoxicity test.

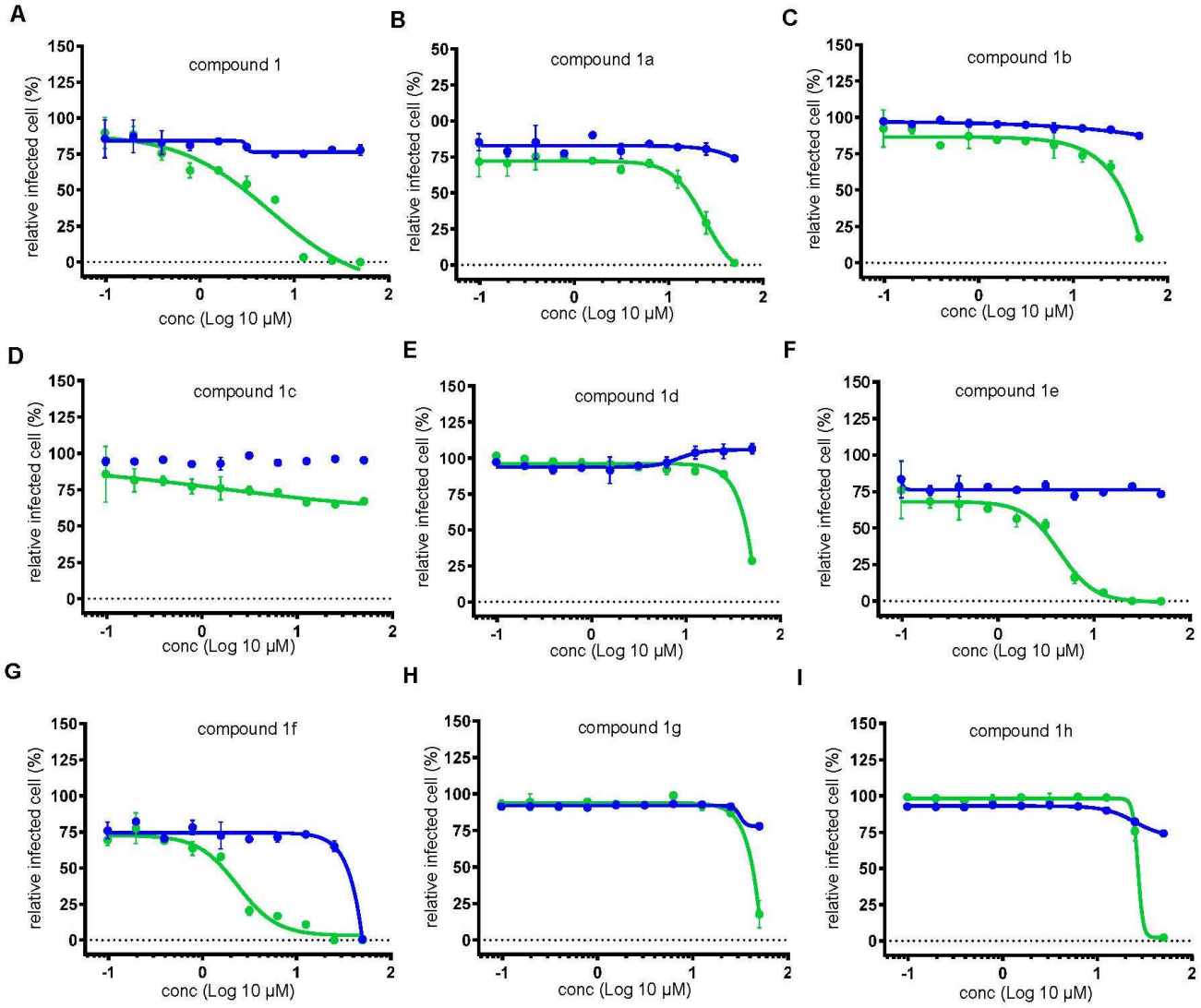

Figure S3. Efficacy measurement of thiophenes (compound 1) against MERS-CoV using immunofluorescence-based infection assay in cell model (related to Figure 3).
Efficacy and cytotoxicity measurements of **1** (**A**) and its analogs (**B-I**). Green dots represent relative infection rate, while blue dots represent relative cytotoxicity at various compound concentrations. Each data point represents the mean of duplicate assays with ±SD.

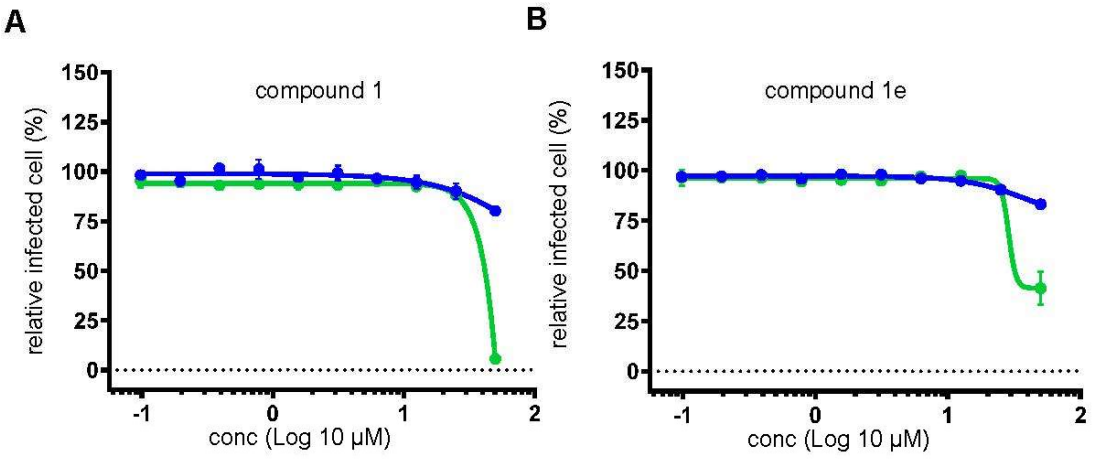

C

Compound	PLpro protease assay		SARS-CoV infection assay		
	MERS-PLpro IC_{50} (μM)	SARS-PLpro IC_{50} (μM)	EC_{50} (μM)	CC_{50} (μM)	SI
1	14.2	156.3	>50	>50	1.00
1e	11.6	146.8	48.27	>50	1.04

Figure S4. Efficacy measurement of compound 1 and 1e in SARS-CoV infection cell model (related to Figure 3).
(A, B) Efficacy measurement of compound **1 (A)** and **1e (B)** against SARS-CoV infection using immunofluorescence-based infection assay in cell model. Green and blue curve show efficacy and toxicity, respectively. Each data point represents the mean of duplicate assays with ±SD. **(C)** Calculation of IC_{50} and EC_{50}. IC_{50} values were calculated from data generated by *in vitro* PLpro protease assay, while EC_{50}, CC_{50}, and SI were calculated from the data obtained by immunofluorescence-based infection assay.

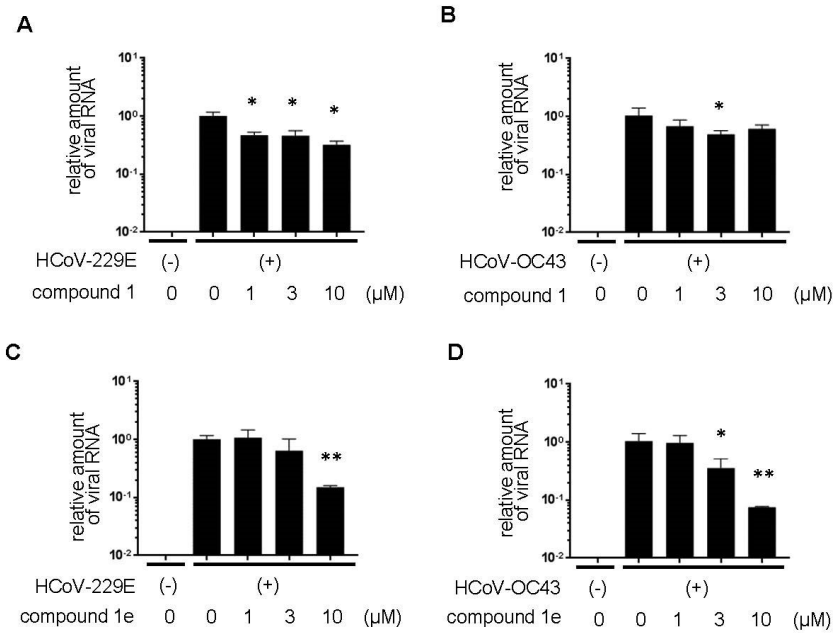

Figure S5. Efficacy measurement of compound 1 and 1e against HCoV-229E or HCoV-OC43 infection in cell model (related to Figure 3).

(A, B) Efficacy of compound **1** against HCoV-229E **(A)** and HCoV-OC43 **(B)** infection measured by quantification of viral RNA. **(C, D)** Efficacy of compound **1e** against HCoV-229E **(C)** and HCoV-OC43 **(D)** infection measured by quantification of viral RNA. Each data point represents the mean of duplicate assays with ±SEM. **p*<0.5, ***p*<0.01, ****p*<0.001 compared to no compound (0 μM) control by Student's *t*-test.

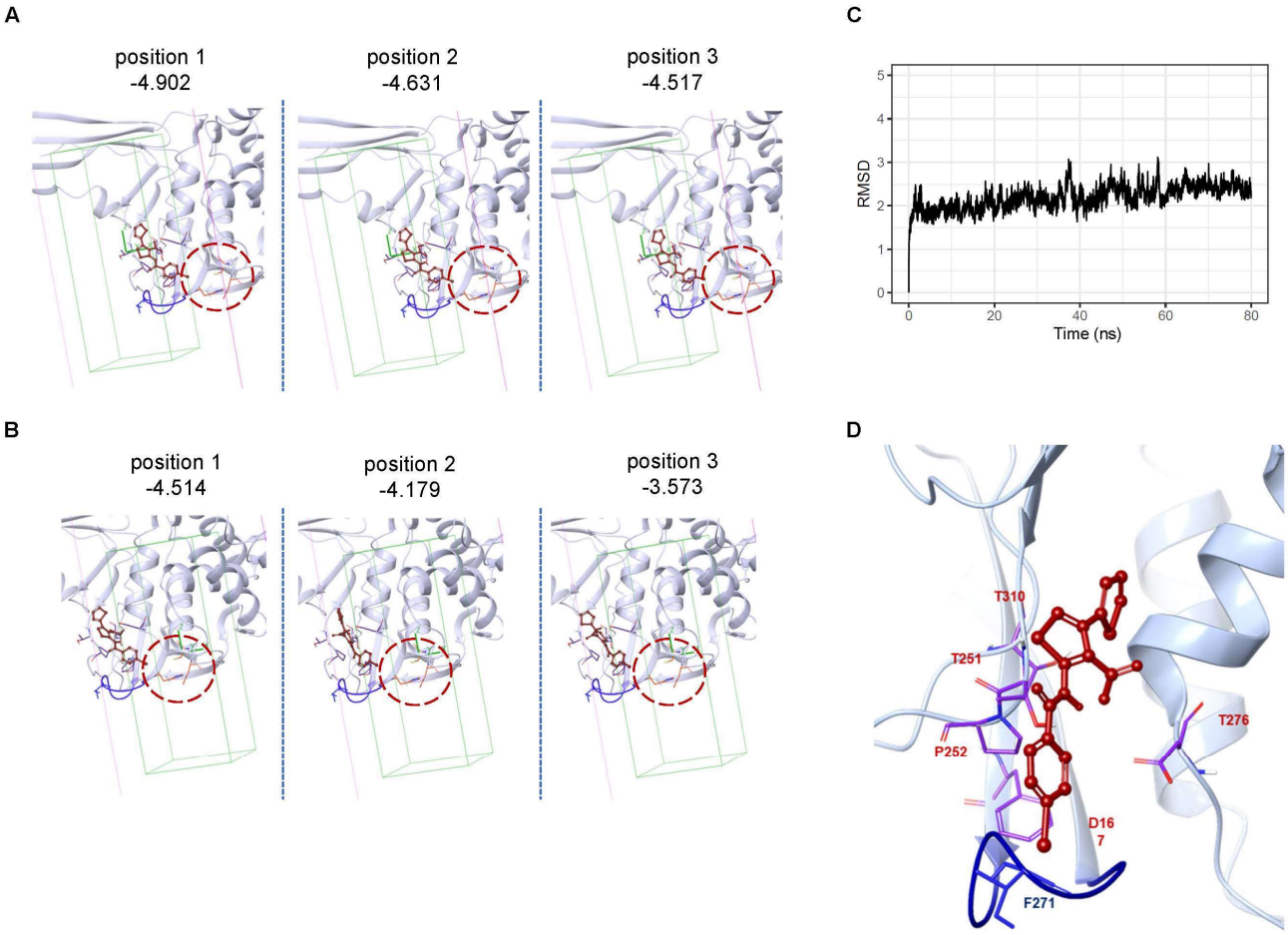

Figure S6. Determination of top 3 binding poses upon docking compound 1 to MERS-PLpro using different residues as a center (related to Figure 3).
(**A**, **B**) Top 3 binding poses generated by docking compound **1** to MERS-PLpro with T251 of the region near BL2 loop as a center (**A**) or C112 of the catalytic site as a center (**B**). Results demonstrate that compound **1** does not bind to the catalytic site even when the docking was performed with the catalytic site as a center. The catalytic site is marked by a red circle. The numbers represent the binding score of each pose. **(C, D)** Result of molecular dynamics simulation (MDS) performed with MERS-PLpro and compound **1** using Cresset's Flare 6.0.1. MDS was performed for 80 ns. Root mean square deviation (RMSD) during the MDS was plotted (**C**) and docking pose at 80 ns was presented (**D**).

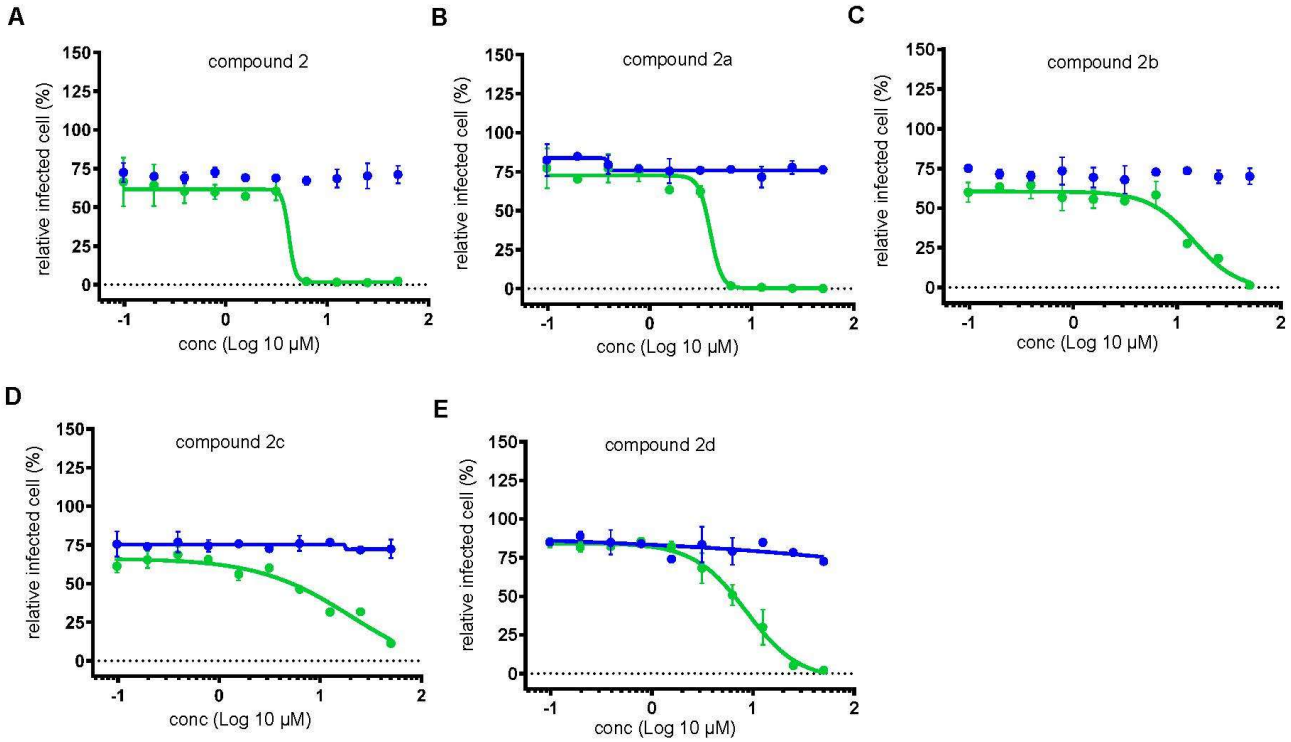

Figure S7. Efficacy measurement of furans (compound 2) against MERS-CoV infection using infection assay in cell model (related to Figure 4).
Efficacy and cytotoxicity measurements of **2** (**A**) and its analogs (**B-E**). Green dots represent relative infection rate, while blue dots represent relative cytotoxicity at various compound concentrations. Each data point represents the mean of duplicate assays with ±SD.

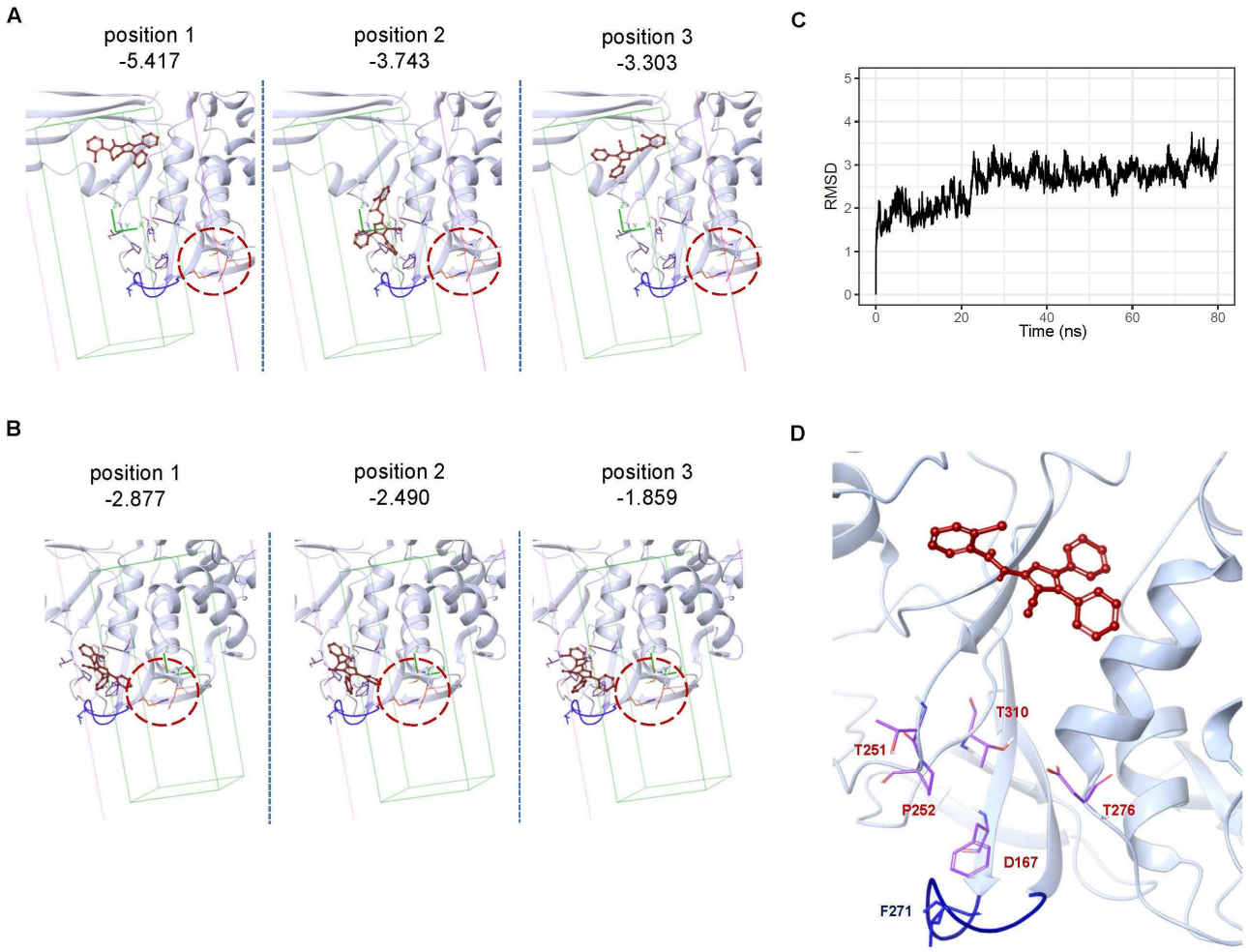

Figure S8. Determination of top 3 binding poses upon docking compound 2 to MERS-PLpro (related to Figure 4).

(**A**, **B**) Top 3 binding poses generated by docking compound **2** to MERS-PLpro with T251 of the region near BL2 loop as a center (**A**) or C112 of the catalytic site as a center (**B**). Results demonstrate that compound **2** does not bind to the catalytic site even when the docking was performed with the catalytic site as a center. The catalytic site is marked by a red circle. The numbers represent the binding score of each pose. **(C, D)** Results of MDS (molecular dynamics simulation) performed with MERS-PLpro and compound **2** for 80 ns using Cresset's Flare 6.0.1. The profile of RMSD (root mean square deviation) during MDS was plotted (**C**) and the docking pose at 80 ns was presented (**D**).

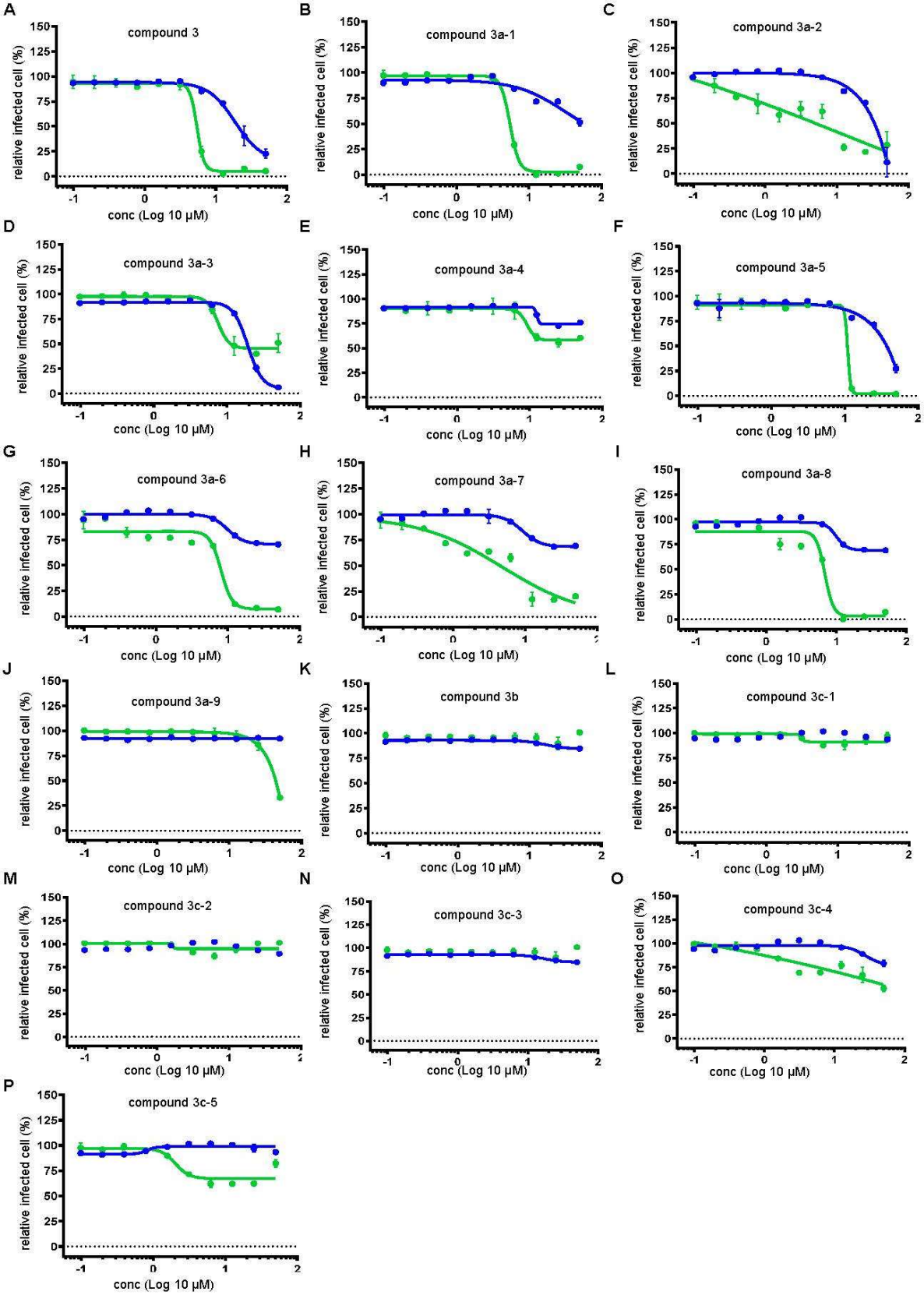

Figure S9. Efficacy measurement of triazoloquinazolines (compound 3) against MERS-CoV infection using immunofluorescence-based infection assay in cell model (related to Figure 5).
Efficacy and cytotoxicity measurements of **3** (**A**) and its analogs (**B-P**). Green dots represent relative infection rate, while blue dots represent relative cytotoxicity at various compound concentrations. Each data point represents the mean of duplicate assays with ±SD.

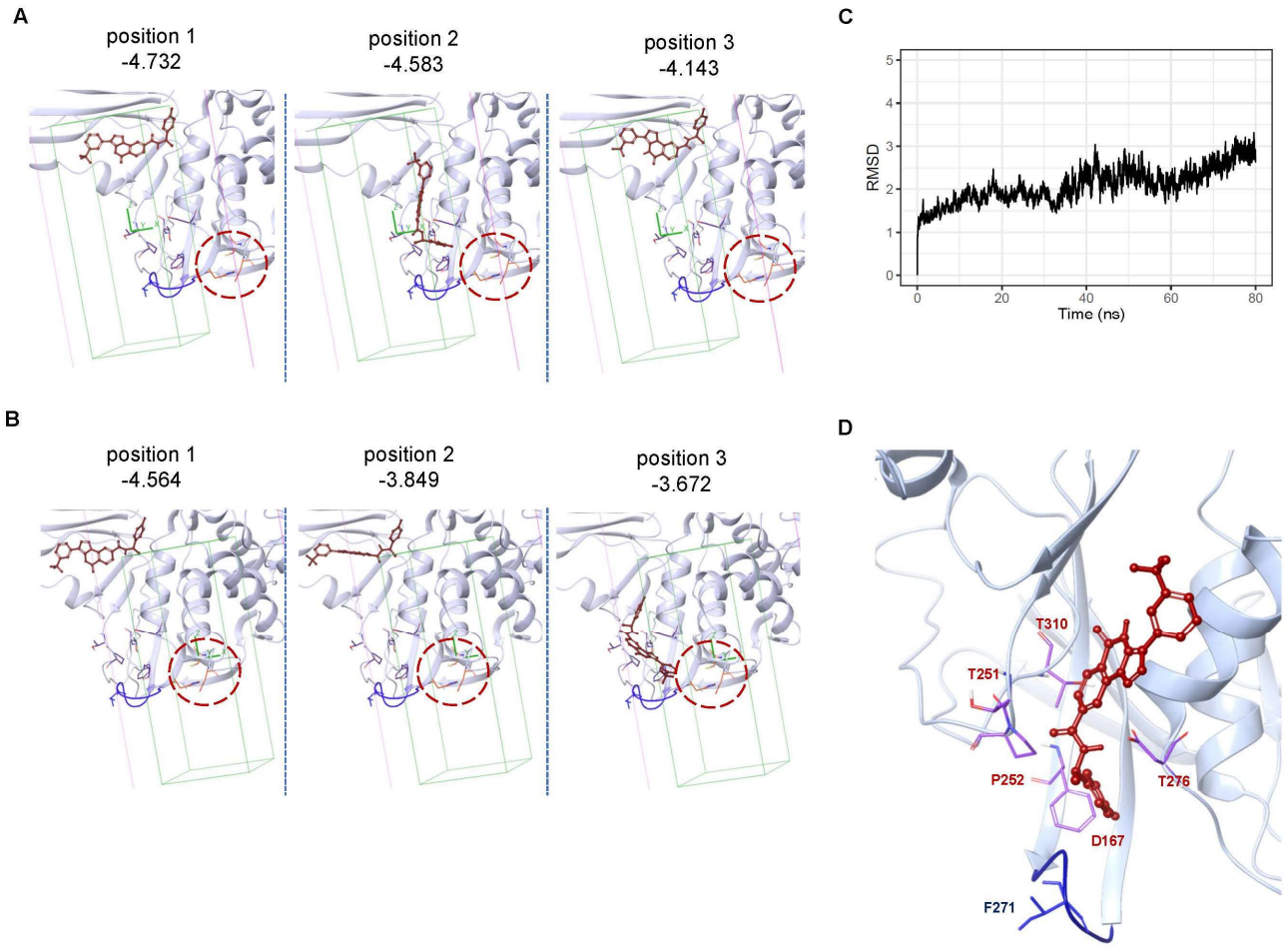

Figure S10. Determination of top 3 binding poses upon docking compound 3 to MERS-PLpro (related to Figure 5).
(**A**, **B**) Top 3 binding poses generated by docking of compound **3** to MERS-PLpro with T251 of the region near BL2 loop as a center (**A**) or C112 of the catalytic site as a center (**B**). Results demonstrate that compound **3** does not bind to the catalytic site. The catalytic site is marked by a red circle. The numbers represent the binding score of each pose. **(C, D)** Results of MDS (molecular dynamics simulation) performed with MERS-PLpro and compound **3** for 80 ns using Cresset's Flare 6.0.1. **(C)** The RMSD (root mean square deviation) during MDS was calculated and plotted. (**D**) The docking pose of compound **3** at 80 ns was presented.

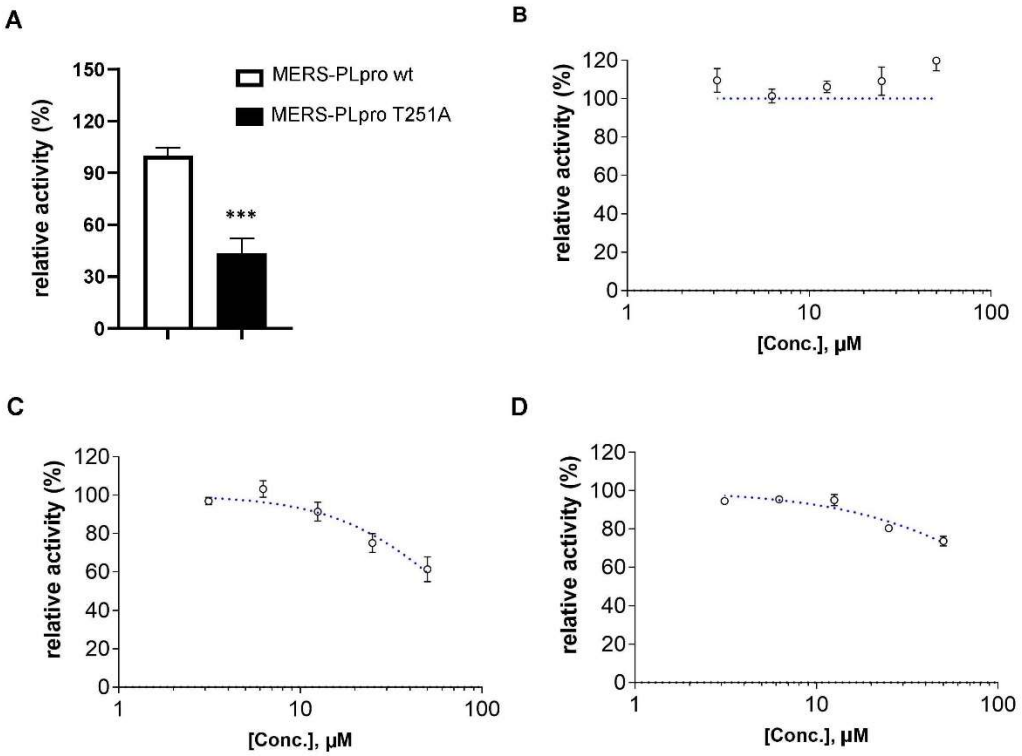

Figure S11. Mutation in T251 residue of MERS-PLpro resulted in loss of enzyme activity and reactivity to thiophene (related to Figure 3, Figure 4, and Figure 5).
(**A**) Enzyme activity of MERS-PLpro with mutation at T251 residue (MERS-PLpro T251A). Substitution of T251 with alanine resulted in a significant loss of its enzyme activity when compared with the wild-type control MERS-PLpro (MERS-PLpro wt). (**B-D**) Potency of compounds against MERS-PLpro T251A. Compounds **1** (**B**), compound **2** (**C**), and compound **3** (**D**) were tested at 0, 3.12, 6.25, 12.5, 25, and 50 μM for their potency against MERS-PLpro T251A. Each data point represents the mean of triplicate assays with ±SEM. **p*<0.5, ***p*<0.01, ****p*<0.001 compared to wild-type MERS-PLpro by Student's *t*-test.

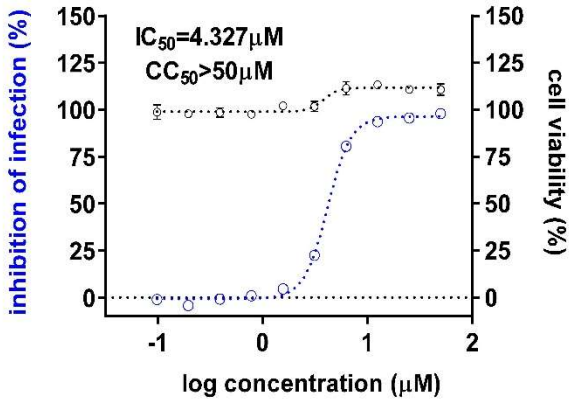

Figure S12. Efficacy and cytotoxicity of remdesivir measured by virus infection assay (related to Figure 6).

Ten different concentrations of remdesivir were tested by the immunofluorescence assay, and IC_{50} and cytotoxicity were calculated through curve fitting analysis using Prism 6. Each data point represents the mean of duplicate assays with ±SD.

Compound	Vendor ID	Vendor
1	Lead compound	Screen library
1a	7114072	ChemBridge
1b	7119694	ChemBridge
1c	D304-0025	ChemDiv
1d	5900099	ChemBridge
1e	5889373	ChemBridge
1f	7112485	ChemBridge
1g	MolPort-004-297-411	MolPort
1h	5895218	ChemBridge
2	Lead compound	Screen library
2a	7744029	ChemBridge
2b	7934758	ChemBridge
2c	7937442	ChemBridge
2d	7940498	ChemBridge
3	Lead compound	Screen library
3a-1	E543-0745	ChemDiv
3a-2	E543-0755	ChemDiv
3a-3	E543-0737	ChemDiv
3a-4	E543-0773	ChemDiv
3a-5	E543-0740	ChemDiv
3a-6	E543-0733	ChemDiv
3a-7	E543-0763	ChemDiv
3a-8	E543-0766	ChemDiv
3a-9	C200-8702	ChemDiv
3b	E543-0720	ChemDiv
3c-1	E543-0394	ChemDiv
3c-2	E543-0720	ChemDiv
3c-3	E543-0443	ChemDiv
3c-4	E543-0198	ChemDiv
3d	E543-0001	ChemDiv

Figure S13. Lead compounds and their analogues used for structure-activity relationship (SAR) studies (related to STAR* methods). List of the vendor ID's and source libraries of the lead compounds (compounds **1**-**3**) and their analogs.